Available online at www.sciencedirect.com
SCIENCE DIRECT®
International Journal of Thermal Sciences 42 (2003) 239–253
International Journal of Thermal Sciences
www.elsevier.com/locate/ijts

Investigation of the prechamber geometrical configuration of a natural gas spark ignition engine for cogeneration: part II. Experimentation

R.P. Roethlisberger, D. Favrat *

Laboratory for Industrial Energy Systems, Swiss Federal Institute of Technology of Lausanne, CH-1015 Lausanne, Switzerland

Received 7 September 2001; accepted 19 April 2002

Abstract

The operation of a small size cogeneration gas engine (6 cylinders, 122 mm bore, 142 mm stroke) modified for unscavenged prechamber ignition was experimentally investigated. The objective was to evaluate the potential to reduce the exhaust gas emissions, particularly the CO emissions, below the Swiss limits (NO_X and CO emissions: 250 and 650 $mg{\cdot}m_N^{-3}$, 5% O_2, respectively), without exhaust gas after treatment, through variations of the prechamber geometrical configuration (size, number, distribution and orientation of the nozzle orifices and prechamber internal volume and shape). The results indicate that trends which increase the penetration of the gas jets and/or promote an early arrival of the flame front at the piston top land crevice entrance (small total nozzle orifice cross sectional area, limited number of nozzle orifices, an orientation of the nozzle orifices towards the squish region, relatively large prechamber internal volume) are beneficial to reduce the CO and THC emissions. Further, these trends mainly result in a slight increase in fuel conversion efficiency.

Keywords: Gas engine; Spark ignition; Unscavenged prechamber; Natural gas; Cogeneration; Emissions; Experimentation

1. Introduction

The motivation of the investigation of an unscavenged prechamber for application on a small size cogeneration gas engine has already been presented in the first part (I [1]) of this publication. The first part shows the results of a numerical simulation performed with *KIVA-3V*. The simulation was performed to assist the selection of the most promising prechamber geometrical configurations for experimentation and to help the interpretation of the experimental results. The second part (II) forming the present paper, presents and discusses the experimental results. It illustrates the influence of the number, size, distribution and orientation of the nozzle orifices as well as the prechamber internal volume and shape on the engine performance and emissions.

2. Engine specifications and experimental conditions

2.1. Engine specifications

The engine used is derived from a *Liebherr* heavy duty diesel engine type 926 converted for natural gas operation on the *Otto* principle and is intended for cogeneration applications. The main engine specifications are summarised in Table 1. The engine is equipped with new cylinder heads, which enable the fitting of spark plugs at the location of the diesel injectors. The combustion chamber was adapted to the spark ignition operation through a modification of the piston geometry and a reduction of the volumetric compression ratio from 17.2 to 12.0 (Fig. 1(a)). Further, the engine is equipped with cylinder liners characterised by a reduced dead volume at the level of the cylinder head gasket to limit the carbon monoxide and hydrocarbons exhaust gas emissions [3–5]. The engine is turbocharged and intercooled. In order to preserve more energy for the turbocharger, the engine is equipped with an insulated exhaust manifold. More detailed information on the engine conversion is given in [6].

* Corresponding author.
E-mail address: daniel.favrat@epfl.ch (D. Favrat).
URL address: http://leniwww.epfl.ch (D. Favrat).

1290-0729/02/$ – see front matter
doi:10.1016/S1290-0729(02)00024-8

Nomenclature

A_n	total nozzle orifice area	mm^2
COV	coefficient of variance	
d_n	nozzle orifice diameter	mm
N_n	number of nozzle orifices	
p	pressure	bar
p_{mi}	indicated mean effect. pres.	bar
Q	heat	J
RH	relative humidity	%
V_c	compression volume	mm^3
V_p	prechamber volume	mm^3

Greek symbols

α_n	nozzle orifice mean angle	°
$\Delta\check{h}_0$	volumetric heating value	$kJ{\cdot}m_N^{-3}$
Δp	pressure difference	bar
$\Delta\varphi$	crank angle interval	°
η_f	fuel conversion efficiency	
λ	relative air to fuel ratio	

Subscripts

ABDC	after bottom dead centre
ATDC	after top dead centre
BBDC	before bottom dead centre
BTDC	before top dead centre
cd	combustion duration
hr	heat released
id	ignition delay
L	lower
N	$p = 1.013$ bar, $T = 273.15$ K
0	$p = 1.013$ bar, $T = 298.15$ K

Abbreviations

CA	crank angle
COV	coefficient of variance
ST	spark timing
TDC	top dead centre

Table 1
Main engine specifications

Manufacturer	Liebherr	Intake valve opening	15° CA_{BTDC}
Type	G 926 TI	Intake valve closing	45° CA_{ABDC}
Number of cyl.	6 in line	Exhaust valve opening	54° CA_{BBDC}
Bore	122 mm	Exhaust valve closing	14° CA_{ATDC}
Stroke	142 mm	Swirl ratio [2, Eq. (8.28)]	2.0
Conrod length	228 mm	Vol. compression ratio	12.0
Total swept vol.	9.96 l	Turbocharger	KKK K27 3371 OLAKB
Number of valves	2	Ignition system	Fairbanks Morse IQ 250
Firing order	1-5-3-6-2-4	Spark plugs	Bosch Super F & W6DC

2.2. Prechamber design and integration

A small water cooled prechamber, representing 2 to 3% of the main chamber compression volume, was designed to be housed in the boss of the existing cylinder head used for the spark plug well. The prechamber integrated to the modified cylinder head is represented in Fig. 1(a). It was designed on a modular basis formed by three parts (nose, body and fixing clamp (not represented on Fig. 1(a))), in order to limit the machining work for the experimental parametric study. Part of the engine water flowing in the cylinder head is derived to cool the nose and the bottom of the body to limit the prechamber and spark plug operating temperature. Several prechamber configurations were realised in order to perform variations of the cross sectional area, number, distribution and orientation of the nozzle orifices, as well as of the prechamber internal volume and shape. The configurations tested were selected on the basis of the results of a CFD numerical simulation with *KIVA-3V*. The configuration which were leading to excessive turbulence intensity or to low fuel concentration at the location of the spark plug electrodes were discarded. The upper limit of turbulence intensity was determined on the basis of the engine cycle-by-cycle variability during the first experiments. The lowest limit of fuel concentration was corresponding to the highest relative air to fuel ratio, which still enables stable operation of the engine with direct spark ignition (i.e., about 1.7). Further details of the prechamber design and cylinder head modifications are given in [6]. The numerical results can be found in[1,6].

2.3. Testing facilities

The experimental investigation was carried out on a test bed especially developed for the study of gas engines (Fig. 2). The test bed is equipped with a direct natural gas supply from the network as well as from an intermediate storage tank at high pressure. The storage tank is used to keep the natural gas composition constant over several series of experiments. The natural gas was supplied from storage and the exact composition was determined by gas chromatography to enable an accurate calculation of the engine fuel conversion efficiency. The composition and the lower heating value of the different natural gas blends used are given in Table 2.

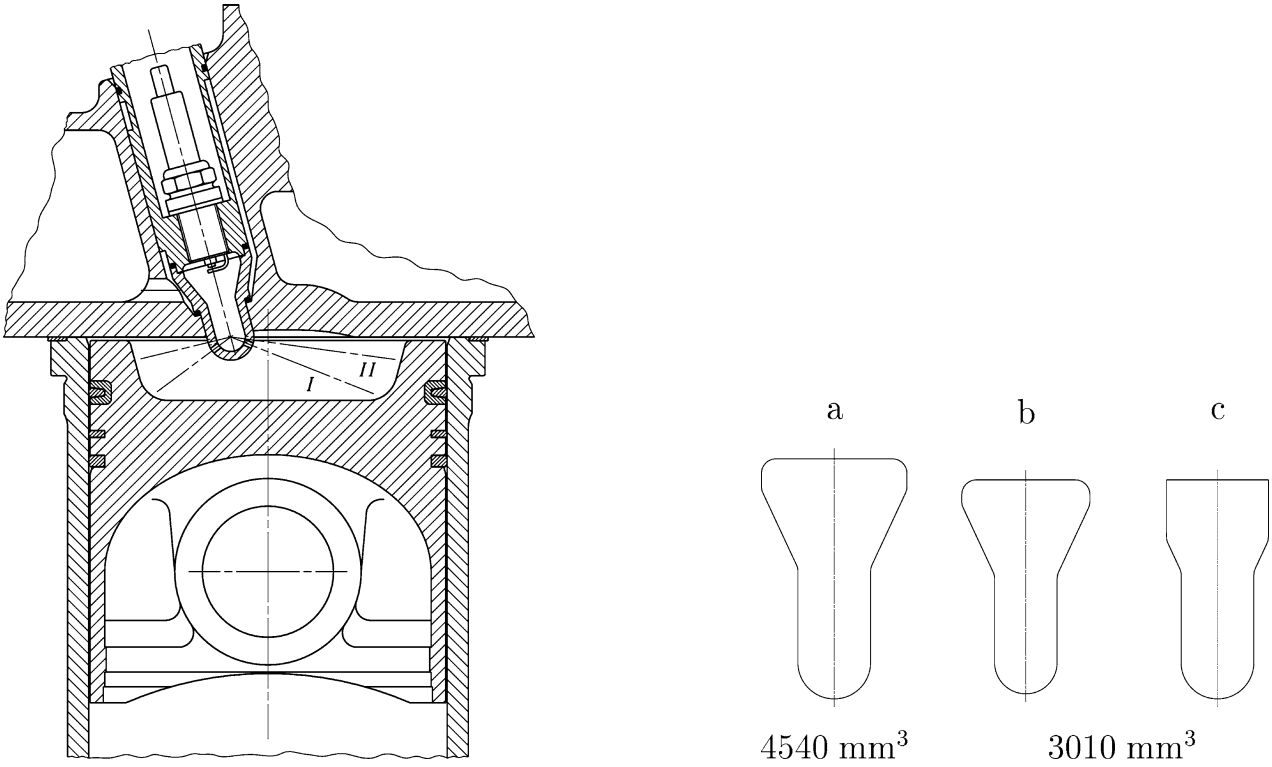

Fig. 1. (a) schematic representation of the combustion chamber with prechamber ignition and original piston for natural gas operation, indicating the two different nozzle orientations studied, (b) shape and volume of the prechamber internal geometries investigated.

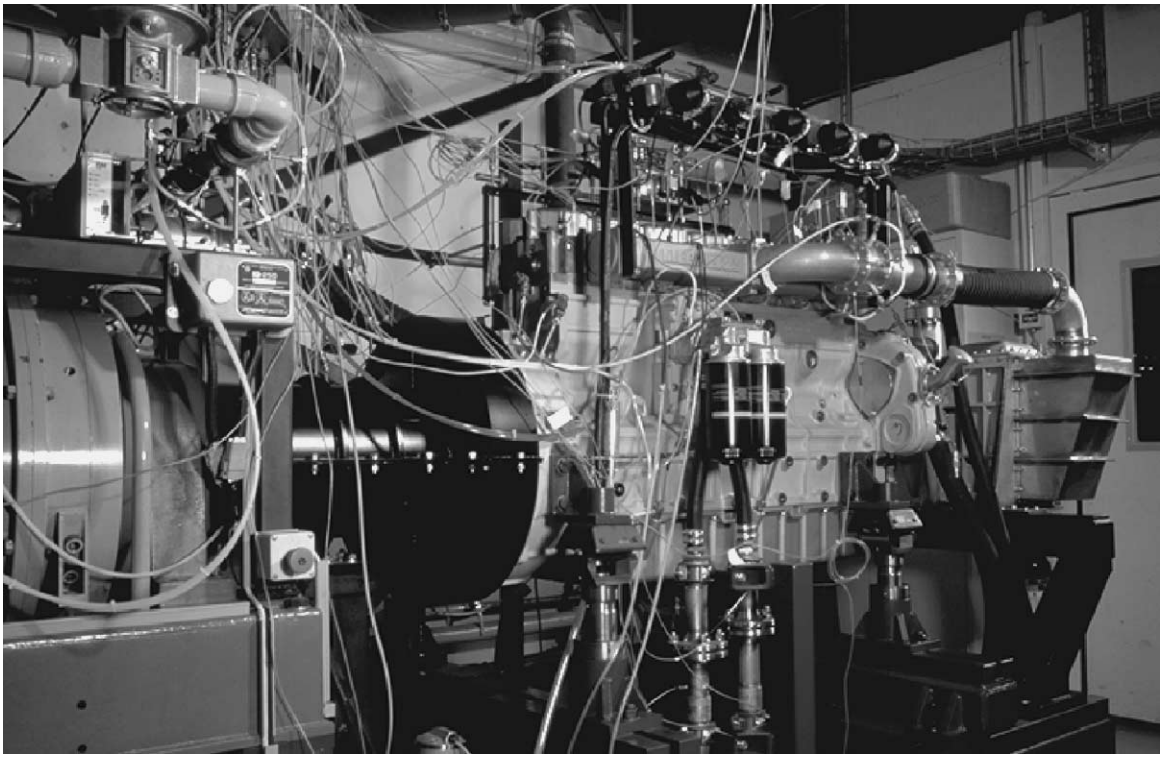

Fig. 2. Test bed with gas engine *Liebherr G 926 TI.*

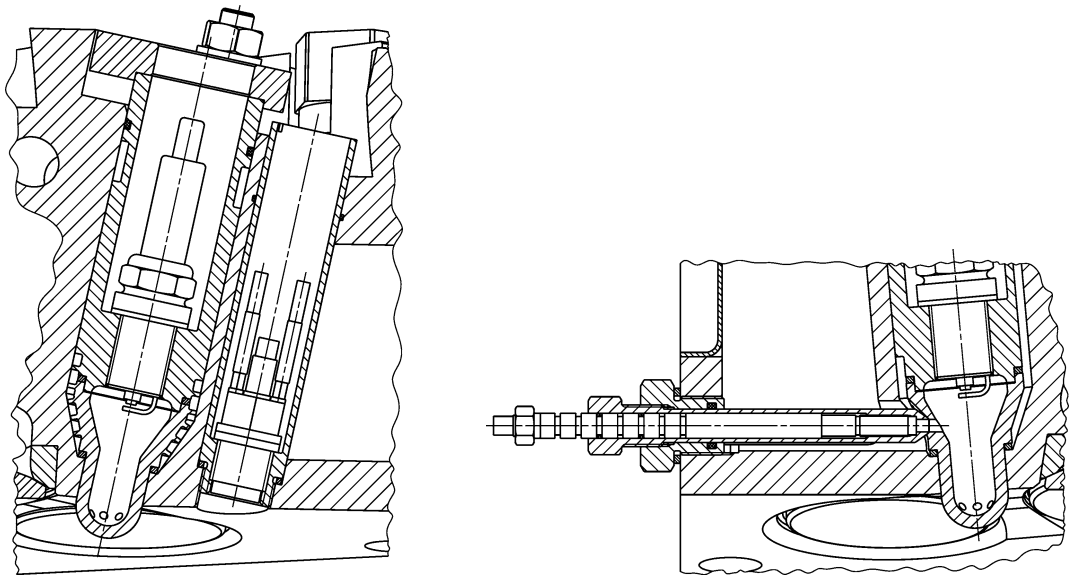

(a) (b)

Fig. 3. Instrumentation for high pressure indication: (a) in main combustion chamber with water cooled piezoelectric transducer *KISTLER 7061B*, (b) in prechamber with piezoelectric tranducer *KISTLER 6053Csp90*.

Table 2
Chemical composition and properties of the natural gas blends used

		NG4	NG5	NG6
CH_4	% vol.	93.01	95.68	96.06
C_2H_6	% vol.	3.28	1.76	1.70
C_3H_8	% vol.	0.84	0.50	0.40
i-C_4H_{10}	% vol.	0.14	0.08	0.07
n-C_4H_{10}	% vol.	0.15	0.09	0.07
i-C_5H_{12}	% vol.	0.04	0.02	0.03
n-C_5H_{12}	% vol.	0.03	0.02	0.01
C_6^+	% vol.	0.04	0.00	0.00
N_2	% vol.	1.84	1.54	1.47
CO_2	% vol.	0.64	0.31	0.19
$\Delta\check{h}_{0,L}$ [a]	$MJ{\cdot}m_N^3$	36.64	36.08	36.05

[a] C_6^+ considered as n-C_6H_{14}.

In addition to the usual pressure, temperature, flow and exhaust gas emission measurements, the cylinders 1 and 3 are instrumented for pressure indication. The corresponding heads were further modified to enable pressure measurement in the pre- and main combustion chamber of cylinder 1 and in the main chamber of cylinder 3. Due to their particular high sensitivity ($\approx$80 $pC{\cdot}bar^{-1}$) and accuracy, water cooled piezoelectric transducers of type *KISTLER 7061B* were chosen for the measurement of the main chamber pressure. Because of the limited accessibility of the prechamber, a piezoelectric transducer of type *KISTLER 6053Csp90* was selected in order to minimise the length of the connecting duct between transducer membrane and prechamber volume, and therefore to limit the amplitude of parasitic pressure oscillations [7]. The implementation of the pressure indication required the development of specific transducer holders, which are represented in Fig. 3. The sealing between the prechamber and the cooling jacket is realised with the direct contact of the spherical surface of the transducer holder tip on a cone machined on the prechamber nose outer surface (Fig. 3(b)). Although the transducer is not externally cooled, the flow of water emerging from the prechamber well limits and stabilises its operating temperature, which reduces the sensitivity shift. Combined with the relatively high sensitivity ($\approx$19 $pC{\cdot}bar^{-1}$) for this size of transducer, this measurement configuration is expected to yield an accurate prechamber pressure indication. The angular measurement resolution is 0.5° CA and the presented results are averaged over 100 engine cycles. The testing facilities and the complete instrumentation have already been described thoroughly elsewhere [3,6].

2.4. Experimental conditions

The experimental conditions are summarised in Table 3. The emission concentration is expressed in $mg{\cdot}m_N^{-3}$ at normal conditions (1013 mbar, 0 °C) and corrected for humidity to 0% RH (dry) and an oxygen (O_2) residual concentration of 5%, corresponding to the Swiss standard. NO_X and total hydrocarbon (THC) are expressed in equivalent NO_2 and CH_4, respectively. The ignition delay ($\Delta\varphi_{id}$) is defined as the difference between the average angular positions where 5% of the heat has been released (start of combustion) and of the spark timing. The combustion duration ($\Delta\varphi_{cd}$) is defined as the difference between the average angular positions where 90% (end of combustion) and where 5% of the heat has been released. The evolution of the pressure in the prechamber is represented through the difference of pressure between the prechamber and the main chamber. The prechamber pressure is corrected in order to obtain the same value in both cham-

Table 3
General experimental conditions

Crankshaft rotational speed	1500 ± 5 rpm
Rated brake mean effective pressure	12 ± 0.1 bar
Rated brake power output	150 ± 1.3 kW
Engine room temperature	29–36 °C
Intake air pressure	980 ± 5 mbar
Intake air temperature	25 ± 0.5 °C
Intake air relative humidity[a]	$50 \pm 0.5\%$
Natural gas pressure[b]	980 ± 5 mbar
Natural gas temperature	14–27 °C
Fuel-air mixture temperature after intercooler	90 ± 1 °C
Exhaust gas pressure after turbocharger	1050 ± 5 mbar
Cooling water inlet temperature	80 ± 0.5 °C
Cooling water mass flow	2.45 ± 0.03 kg·s^{-1}
Lubricating oil inlet temperature	90 ± 0.5 °C
Lubricating oil mass flow	1.21 ± 0.01 kg·s^{-1}

[a] When not otherwise specified.
[b] Through zero pressure regulator controlled by intake air pressure.

bers at intake valve closure. At this particular crank angle, the flow between the chambers is very weak, thus generating no significant pressure drop. Further, the dynamical behaviour of both transducers is expected to be very similar. The emissions of NO_X, CO, THC, O_2 and CO_2 were measured and the relative air to fuel ratio is calculated on the basis of the exhaust gas composition.

3. Results and discussion

This section presents and discusses the influence of the total cross sectional area, number, distribution and orientation of the nozzle orifices, as well as the prechamber internal volume and shape, on the engine performance and emissions.

3.1. Nozzle orifice cross sectional area

The investigation was performed with prechambers featured with an internal volume of 4540 mm^3 and 6 nozzle orifices, unevenly distributed (see Fig. 6) and oriented at an angle of ≈62° from the prechamber axis (orientation I in Fig. 1). Four different total nozzle orifice cross sectional areas were evaluated: $A_n = 9.37, 14.10, 18.85$ and 23.64 mm^2, which corresponds to orifices of diameter 1.41, 1.73, 2.00 and 2.24 mm, respectively. The engine was operated at a constant spark timing of 10.8° CA_{BTDC}.

The results for the four different total nozzle orifice cross sectional areas are represented in Fig. 4. At constant relative air to fuel ratio, the reduction of the total nozzle orifice cross sectional area produces an important increase in the pressure difference between pre- and main chamber (Fig. 4(c)), which is expected to generate stronger gas jets penetrating deeper into the main combustion chamber. Consequently, this significantly accelerates and intensifies the main chamber combustion process (Fig. 4(b)) and results in an important decrease of the combustion duration (Fig. 4(d)). In turn, the intensification and acceleration of the combustion process produces an increase in main chamber pressure (Fig. 4(a)). The prechamber with the smallest total nozzle orifice cross sectional area does not enable the engine operation with a relative air to fuel ratio above 1.62. From this value, prechamber ignition failure occurs at a relatively low frequency, which immediately increases the coefficient of variance of p_{mi} far above the usually admitted maximum value of 5% (only stable operating points were measured). The occasional prechamber ignition failure seems to originate in the higher turbulence intensity at the ignition point, which perturbs the arc discharge and the initial flame kernel generation [8]. The occurrence of ignition instabilities at a low value of relative air to fuel ratio strongly limits the potential to reduce the NO_X emissions (Fig. 4(e)). Therefore, further discussion will essentially concentrate on the three larger cross sectional areas.

When considering the same NO_X emissions, the reduction of the total nozzle orifice cross sectional area leads to similar CO and THC emissions (Fig. 4(e)). This may be explained by the offset of the two following conflicting effects: firstly, the deeper penetration of the gas jets induced by a smaller nozzle orifice cross sectional area tends to reduce the amount of unburnt mixture compressed in the combustion chamber crevices by an early arrival of the flame front at their entrance. Secondly, the intensification of the combustion process by stronger gas jets increases the cylinder pressure. On one hand, this tends to increase the quantity of unburnt mixture flowing into the crevices. On the other hand, it decreases the bulk gases temperature during expansion, which is likely to reduce the proportion of unburnt hydrocarbons transformed into fully oxidised products during the secondary combustion process.

At constant NO_X emissions, a reduction of the area from 23.64 to 18.85 mm^2 yields an increase in fuel conversion efficiency of more than 0.5%-point, but a further reduction from 18.85 to 14.10 mm^2 does not significantly affect the efficiency (Fig. 4(f)). This could be a result of a higher heat transfer to the main combustion chamber wall due the deeper penetration of the gas jets. The total nozzle orifice cross sectional area has no perceptible effect on the cycle-by-cycle variability illustrated by the coefficient of variance of p_{mi}. This seems to indicate that the gain in main chamber combustion stability is balanced by the deterioration of the prechamber ignition conditions due to the increase in turbulence intensity. Finally, the results indicate the existence of an optimal size of the total nozzle orifice cross sectional area which achieves the lowest NO_X emissions. In the case of the nozzle orifice configurations tested, the optimal size is close to 18.85 mm^2.

3.2. Number of nozzle orifices

The investigation was performed with prechambers featured with an internal volume of 4540 mm^3 and orifices unevenly distributed (see Fig. 6) and oriented at an angle of

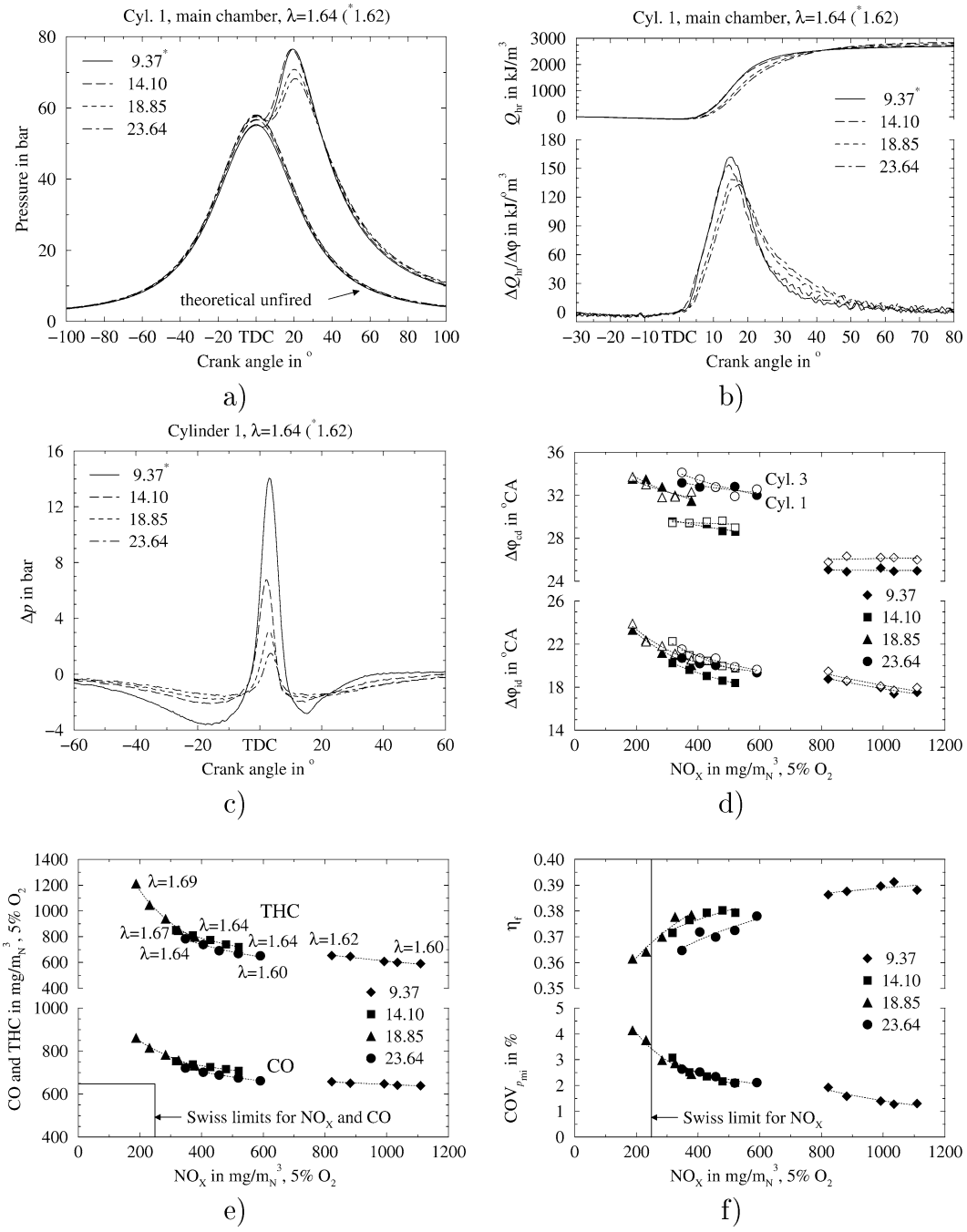

Fig. 4. Influence of the total nozzle orifice cross sectional area on the engine performance and emissions; main chamber pressure (a), main chamber heat-release rate and integral (b) and pressure difference between pre- and main chamber (c) at constant relative air to fuel ratio; ignition delay and combustion duration (d) CO and THC emissions (e) and fuel conversion efficiency and coefficient of variance of p_{mi} (f) as function of NO_X emissions; $V_p = 4540$ mm^3, $N_n = 6$, $\alpha_n \approx 62°$, ST $= 10.8°$ CA_{BTDC}, NG5.

≈62° from the prechamber axis (orientation I in Fig. 1), while keeping a constant total nozzle orifice cross sectional area of 14.10 mm^2. Configurations with 4 and 6 nozzle orifices of diameter 2.12 and 1.73 mm, respectively, were evaluated. The engine was operated at a constant spark timing of 10.8° CA_{BTDC}.

The results corresponding to the two different cases are represented together in Fig. 5. At the same relative air to fuel ratio, the reduction of the number of nozzle orifices from 6 to 4, while keeping a constant total nozzle orifice cross sectional area, does not affect significantly the prechamber combustion process. This is indicated by a similar pressure difference between pre- and main chamber (Fig. 5(c)). Despite a similar prechamber combustion process, the reduction of the number of nozzle orifices yields a slower first part and a faster second part of the main chamber combus-

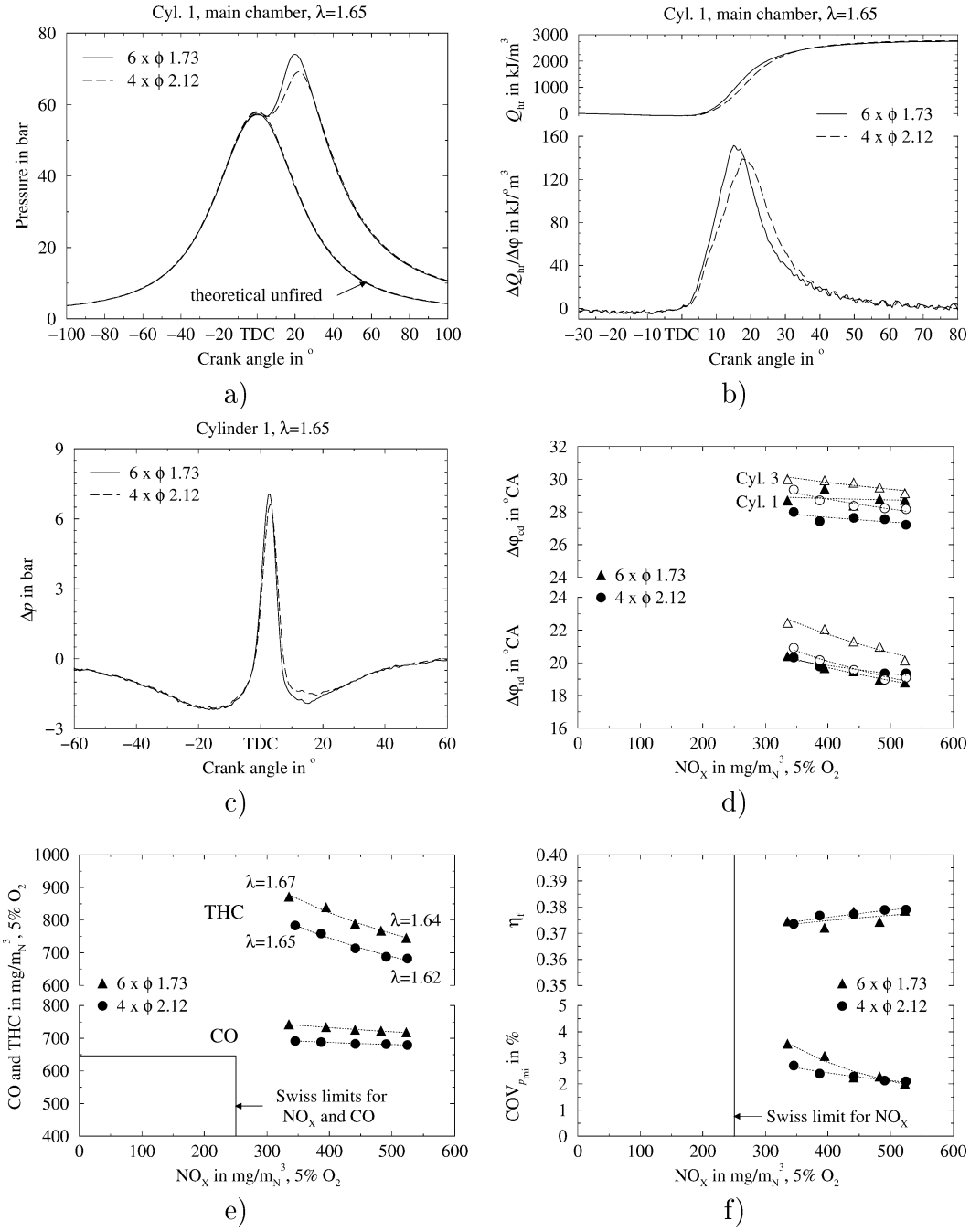

Fig. 5. Influence of the number of nozzle orifices on the engine performance and emissions; main chamber pressure (a), main chamber heat-release rate and integral (b) and pressure difference between pre- and main chamber (c) at constant relative air to fuel ratio; ignition delay and combustion duration (d) CO and THC emissions (e) and fuel conversion efficiency and coefficient of variance of p_{mi} (f) as function of NO_X emissions; $V_{\mathrm{p}} = 4540\ \mathrm{mm}^3$, $A_{\mathrm{n}} = 14.10\ \mathrm{mm}^2$, $\alpha_{\mathrm{n}} \approx 62°$, $\mathrm{ST} = 10.8°\ \mathrm{CA}_{\mathrm{BTDC}}$, NG5.

tion process (Fig. 5(b)). The second part over-compensates the effect of the slower first part, which results in a slight reduction of the combustion duration (Fig. 5(d)). Further, the change in the rate of heat-release induces a shift of the centre of gravity of the combustion into the expansion phase. The reduction of the number of orifices decreases the number of main chamber distributed ignition sources and may explain the lower rate of heat released during the first part of the main chamber combustion process. The acceleration of the second part of the combustion process is likely to be due to a significant increase of the initial main chamber flame front surface. This would support the assumption that the reduction of the number of nozzle orifices increases the size and penetration of the gas jets. The shift of the centre of gravity of the combustion process into the expansion phase results in a significant decrease in main chamber peak cylinder pressure (Fig. 5(a)).

When considering equal NO_X emissions, the moderate decrease in combustion duration associated with the reduction from 6 to 4 orifices yields a slight increase in fuel conversion efficiency (Fig. 5(f)). The transition from 6 to 4 orifices results in reduction of ≈5% and ≈9% of the CO and THC emissions, respectively (Fig. 5(e)). This may originate in the two following effects. On one hand, the lower cylinder pressure (Fig. 5(a)) tends to reduce the amount of unburnt mixture compressed into the combustion chamber crevices. On the other hand, the expected deeper penetration of the gas jets should enable the flame front to reach earlier the cylinder head gasket and piston top land crevice entrances. Both effects tend to reduce the amount of unburnt mixture escaping the primary oxidation.

Finally, the transition from 6 to 4 orifices leads to a significant improvement of the cycle-by-cycle variability, particularly at low NO_X emissions. However, despite the better engine operating stability with 4 nozzle orifices, the relative air to fuel ratio could not be increased beyond 1.65 in order to further reduce the NO_X emissions. Above this value, ignition failure started to occur. This phenomenon is not related to the change in prechamber configuration but to the particular spark plug used. This problem is discussed in detail in the next section.

3.3. Nozzle orifice distribution

The azimuthal orientation of the nozzle orifices was established in order to achieve a relatively uniform distribution of the gas jets into the main combustion chamber. Due to the tilted prechamber position and its location set off from the main combustion chamber axis, this led to an uneven distribution of the nozzle orifices around the prechamber nose (Fig. 6(a)). In order to evaluate the influence of the nozzle orifice distribution on the combustion process, a set of prechambers with an even distribution (Fig. 6(b)) and an orientation of 60° of the orifices (axisymetrical prechamber nose) was manufactured and tested on the engine. The investigation was performed with prechambers featured with an internal volume of 4540 mm^3 and 6 nozzle orifices of diameter 1.73 mm ($A_n = 14.10$ mm^2). The engine was operated at a constant spark timing of 10.8° CA_{BTDC}.

The results discussed in this section are showed in Fig. 7. Like in the other sections, only the evolution of the pressure and the heat-release rate and integral during the engine cycle of cylinder 1 are presented. However, unlike in the other sections, the results associated to cylinder 3 do not show the same trend and indicate no significant influence of the distribution of the nozzle orifice. This consequently limits the possible interpretation of the results.

At constant relative air to fuel ratio, the transition from uneven to even nozzle orifice distribution does not affect significantly the prechamber flow dynamics and combustion process (Fig. 7(c)). The large difference in ignition delay between cylinder 1 and 3 in the case of the uneven nozzle

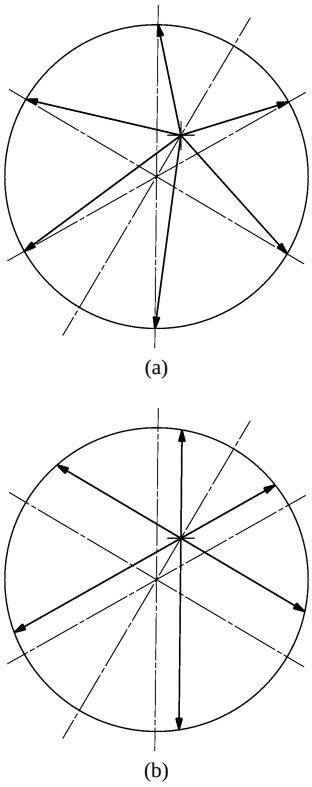

Fig. 6. Theoretical path of the gas jet generated by the nozzle orifice distribution around the prechamber nose: (a) uneven, (b) even.

orifice distribution (Fig. 7(d)) makes it difficult to evaluate the influence of the nozzle orifice distribution on the main chamber combustion process. However, the even distribution of nozzle orifices clearly leads to a decrease of ≈2° CA of the combustion duration in both cylinders.

When considering same NO_X emissions, the somewhat faster combustion associated with the even nozzle orifice distribution (Fig. 7(d)) yields a moderate increase in fuel conversion efficiency of ≈0.5%-point (Fig. 7(f)). However, the even nozzle orifice distribution results in a higher cycle-by-cycle variability. For equal NO_X emissions, the even nozzle orifice distribution yields somewhat higher CO and THC emissions (Fig. 7(f)). Two different phenomena could contribute to this result. On one hand, the lower concentration of the gas jets in the main combustion chamber region characterised by the largest distance between prechamber nose and cylinder wall (compare Fig. 6(a) and (b)) may delay the flame front arrival at the remotest location of the piston top land and cylinder head gasket crevice entrances. On the other hand, the higher cycle-by-cycle variability (Fig. 7(f)) may indicate an increase of the frequency of bulk gas quenching. Both phenomena tend to increase the amount of unburnt mixture escaping the primary oxidation process.

The engine operation with the even nozzle orifice distribution is characterised by a higher cycle-by-cycle variability which cannot directly be explained on the basis of the experimental results. As identified during a later test, the degra-

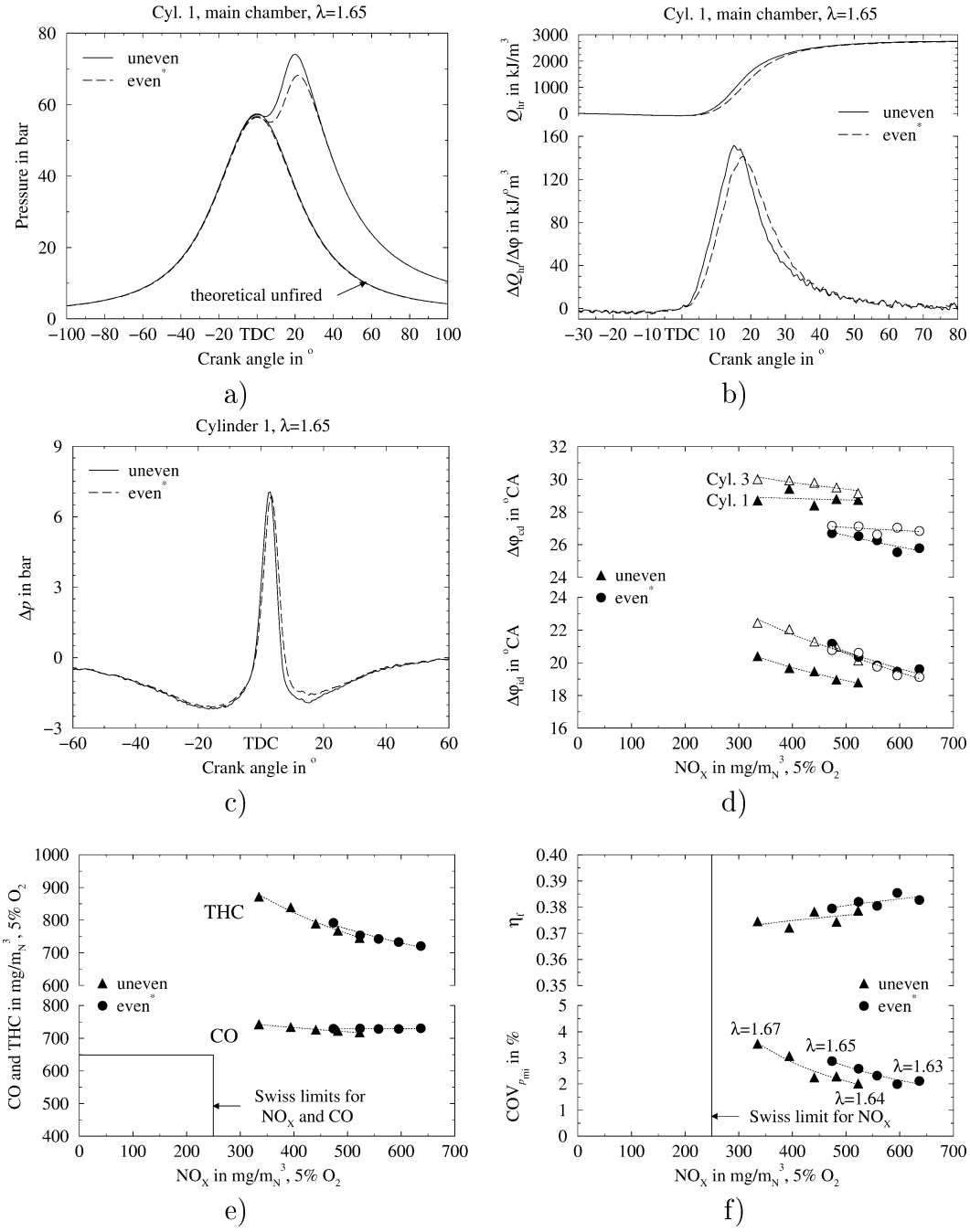

Fig. 7. Influence of the nozzle orifice distribution on the engine performance and emissions: main chamber pressure (a), main chamber heat-release rate and integral (b) and pressure difference between pre- and main chamber (c) at constant relative air to fuel ratio; ignition delay and combustion duration (d) CO and THC emissions (e) and fuel conversion efficiency and coefficient of variance of p_{mi} (f) as function of NO_X emissions; $V_{\mathrm{p}} = 4540\ \mathrm{mm}^3$, $N_{\mathrm{n}} = 6$, $A_{\mathrm{n}} = 14.10\ \mathrm{mm}^2$, $\alpha_{\mathrm{n}} \approx 78°$ ($* = 60°$), $\mathrm{ST} = 10.8°\ \mathrm{CA}_{\mathrm{BTDC}}$, NG5.

dation of the combustion stability seems to mainly originate in the particular evolution of the spark plug behaviour after several tens of operating hours, causing an increase in the frequency of ignition failure. The replacement of the spark plugs by new ones dramatically improved the engine operating stability. Small spark plugs *Bosch Super* type *F6DC* were selected because of the limited space available in the original cylinder head. Consequently, the following experiments were first carried out with spark plugs not exceeding ten operating hours and then were replaced by standard spark plugs type *W6DC*, characterised by the same electrode configuration and thermal index. However, the fitting of the standard spark plugs required the milling of the tightening hexagon from 21 to 19 mm.

At constant NO_X emissions, the use of an even nozzle orifice distribution in comparison to an uneven distribution leads to a slight increase in fuel conversion efficiency, while producing only slightly higher CO and THC emissions. However, the results presented in the previous section indicate that a prechamber with 4 nozzle orifices enables a significant reduction of the CO and THC emissions, while not affecting the fuel conversion efficiency. When now considering a lower number of nozzle orifices, it appears even more important to obtain a uniform distribution of the gas jets in the main combustion chamber. Therefore and because the general trend will be to use 4 nozzle orifices, only the uneven distribution was used for the next prechamber configurations.

3.4. Nozzle orifice orientation

The two different orientations of the nozzle orifices indicated in Fig. 1 were investigated. The first orientation (I), characterised by an average angle from the prechamber axis of $\approx 62°$, yields a relatively uniform distribution of the gas jets issuing from the prechamber into the volume of unburnt mixture located in the main chamber when the piston is close to TDC. The second orientation (II), with an average angle of $\approx 78°$, aims to promote an early arrival of the flame front in the squish region, in order to reduce the amount of unburnt mixture compressed in the cylinder head gasket and piston top land crevices. The investigation was carried out with prechambers featured with an internal volume of 4540 mm^3 and 6 nozzle orifices of diameter 2.00 mm ($A_n = 18.85$ mm^2), unevenly distributed. The engine was operated at a constant spark timing of 8.3° CA_{BTDC}. The overall low cycle-by-cycle variability associated with the prechamber ignition operation enables a further delay of the spark timing, which permits to take advantage of its beneficial influence on the NO_X and CO emissions. Therefore, the spark timing was retarded from 10.8 to 8.3° CA_{BTDC} for the remaining prechamber configuration parameters.

The results corresponding to the two different nozzle orifice orientations are given in Fig. 8. The transition from orientation I to II leads to a perceptible intensification of the prechamber combustion process. This results in a moderate increase of the pressure difference between pre- and main combustion chambers, which occurs somewhat earlier in the engine cycle (Fig. 8(c)). When considering the same relative air to fuel ratio, the higher pressure difference between pre- and main chamber generated by orientation II yields a more rapid main chamber combustion process (Fig. 8(b)). This results in a somewhat shorter ignition delay and a significant decrease in combustion duration (Fig. 8(d)). The slightly shorter ignition delay is expected to originate in somewhat stronger gas jets. In turn, the acceleration of the combustion process causes a slight increase of the maximum cylinder pressure (Fig. 8(a)).

When considering the same NO_X emissions, the significantly shorter combustion duration ($\approx 4°$ CA) combined with the somewhat reduced ignition delay induced by the nozzle orifice orientation II leads to a somewhat higher fuel conversion efficiency (Fig. 8(f)). This orientation yields no perceptible change in cycle-by-cycle variability. Despite the somewhat higher peak cylinder pressure, the orientation of the gas jets towards the squish region results in a reduction of the CO and THC emissions (Fig. 8(e)). The reduction is small with a relatively rich fuel-air mixture, but becomes much larger when the relative air to fuel ratio increases. Further, orientation II induces a fundamental change in the behaviour between CO and THC emissions: the CO emissions slightly decrease with the increase of relative air to fuel ratio (this trend has been established several times), while the THC emissions increase due to the degradation of the combustion stability. These results tend to support the assumption that an early flame front arrival in the squish region reduces the amount of unburnt mixture compressed in the piston top land and cylinder head gasket crevices. Further, the slight decrease of the CO emissions with the increase of relative air to fuel ratio seems to indicate a progressive reduction of the amount of hydrocarbons located in the combustion chamber crevices prior to the flame front arrival. On the other hand, the increase in THC emissions should essentially result from the more frequent occurrence of bulk gas flame quenching.

The orientation of the nozzle orifices towards the squish region simultaneously reduces the THC and CO emissions, particularly when increasing the relative air to fuel ratio to decrease the NO_X emissions. In addition, it also improves somewhat the fuel conversion efficiency. For these reasons, this particular nozzle configuration was adopted to evaluate the influence of the prechamber internal volume and shape, presented in the following two sections.

3.5. Prechamber internal volume

Two different prechamber internal volumes were evaluated. The volumes are 4540 and 3010 mm^3, corresponding to 2.9 and 1.9% of the compression volume (clearance and prechamber volumes), respectively. The internal dimensions of the small prechamber (Fig. 1(b), (b)) corresponds to a proportional reduction of the larger prechamber (Fig. 1(b), (a)), which results in a similar internal shape. In order to achieve approximately the same orifice flow conditions (i.e., pressure drop), the ratio between the nozzle orifice total cross sectional area and the prechamber internal volume was kept constant to a value of $A_n/V_p = 0.0042$ mm^{-1}. This results in nozzle orifice diameters of 2 and 1.63 mm for prechamber *a* and *b*, respectively. The specific parameters of each prechamber are summarised in Table 4. The investigation was performed with prechambers featured with 6 nozzle orifices unevenly distributed and oriented at $\approx 78°$. The engine was operated at a constant spark timing of 8.3° CA_{BTDC}.

The results corresponding to the two different internal volumes are represented together in Fig. 9. At constant relative air to fuel ratio, the small prechamber (b) causes

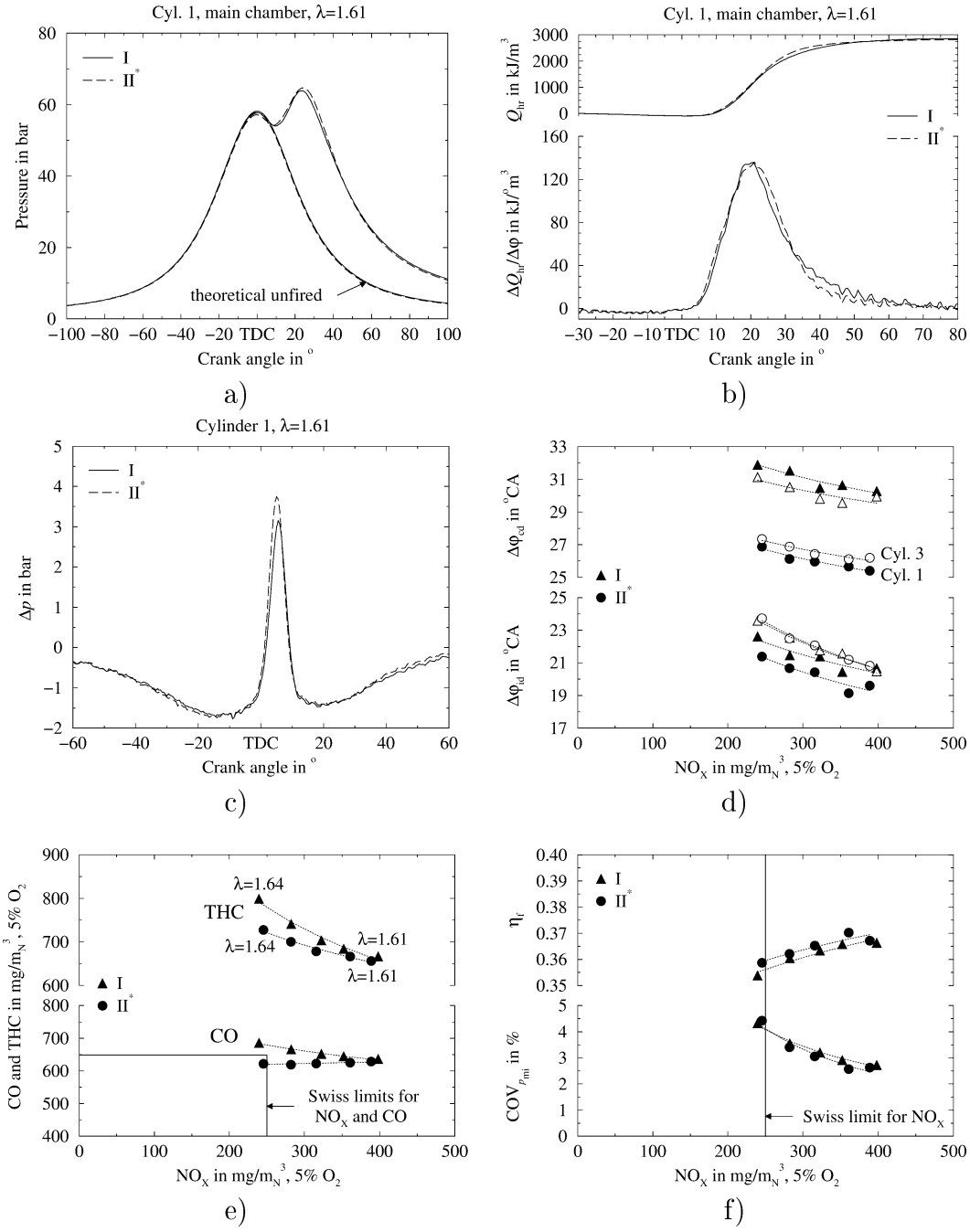

Fig. 8. Influence of the nozzle orifice orientation on the engine performance and emissions: main chamber pressure (a), main chamber heat-release rate and integral (b) and pressure difference between pre- and main chamber (c) at constant relative air to fuel ratio; ignition delay and combustion duration (d) CO and THC emissions (e) and fuel conversion efficiency and coefficient of variance of p_{mi} (f) as function of NO_X emissions; $V_{\mathrm{p}} = 4540\ \mathrm{mm}^3$, $N_{\mathrm{n}} = 6$, $A_{\mathrm{n}} = 18.85\ \mathrm{mm}^2$, RH ≈ 52 (* $= 49$) %, ST $= 8.3°\ \mathrm{CA}_{\mathrm{BTDC}}$, NG6.

Table 4
Prechamber configurations

		a	*b*
V_{p}	mm^3	4540	3010
% V_{c}	–	2.9	1.9
d_{n}	mm	2.00	1.63
N_{n}	–	6	6
A_{n}	mm^2	18.85	12.52

an earlier start of the prechamber combustion, which results in a larger pressure difference between pre- and main chamber (Fig. 9(c)). However, the combination of the smaller prechamber volume and the earlier start of the prechamber combustion process reduces the amount of unburnt mixture flowing into the prechamber. Thus, the small prechamber (b) is expected to generate weaker gas jets, but which are emerging more rapidly and earlier in

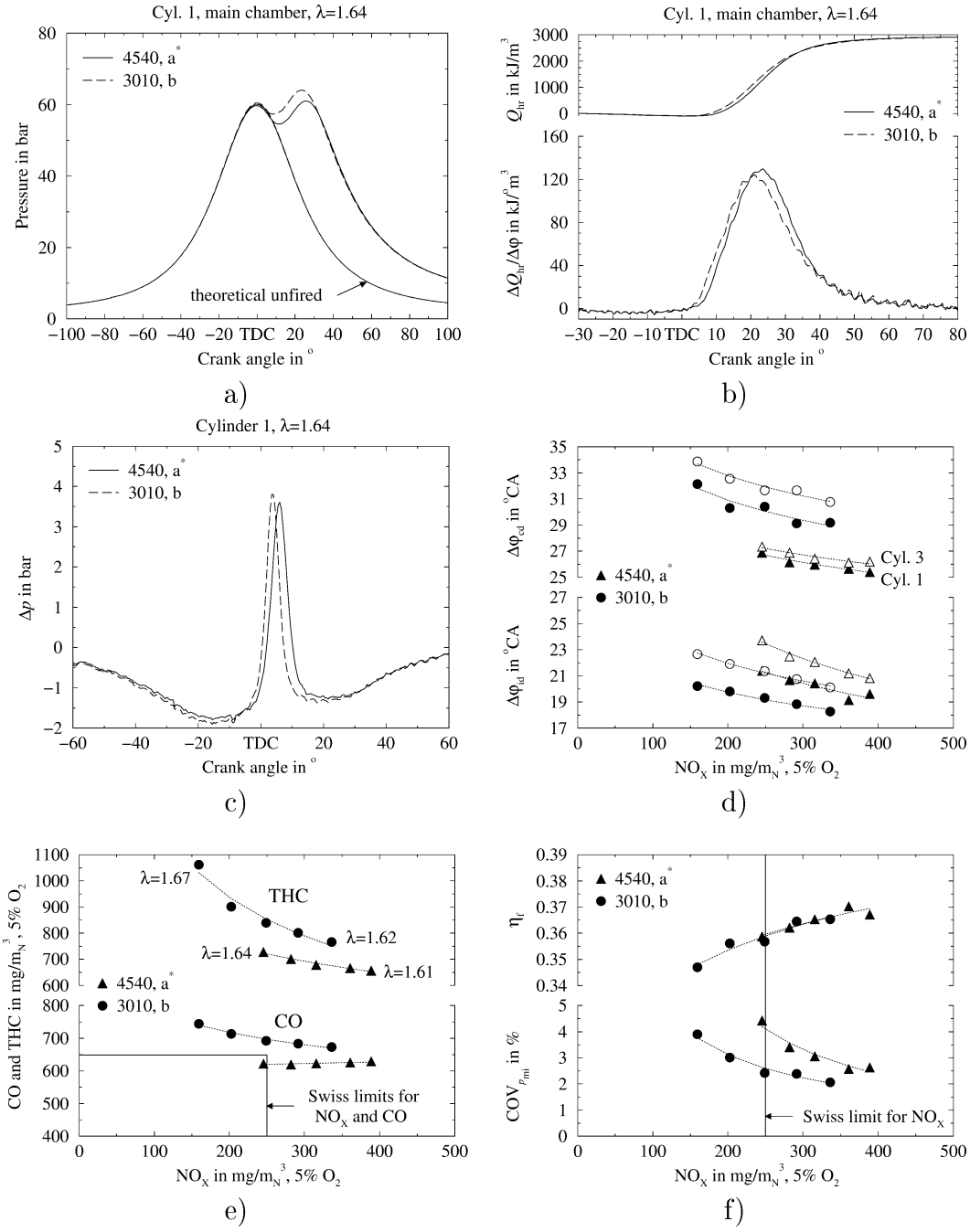

Fig. 9. Influence of the prechamber internal volume on the engine performance and emissions: main chamber pressure (a), main chamber heat-release rate and integral (b) and pressure difference between pre- and main chamber (c) at constant relative air to fuel ratio; ignition delay and combustion duration (d) CO and THC emissions (e) and fuel conversion efficiency and coefficient of variance of p_{mi} (f) as function of NO_X emissions; $A_{\mathrm{n}}/V_{\mathrm{p}} = 0.0042\ \mathrm{mm}^{-1}$, $N_{\mathrm{n}} = 6$, $\alpha_{\mathrm{n}} \approx 78°$, RH ≈ 50 (* $= 49$) %, ST $= 8.3°$ $\mathrm{CA}_{\mathrm{BTDC}}$, NG6.

the engine cycle. This causes a slight reduction of the main chamber ignition delay of approximately 2° CA (Fig. 9(d)) and consequently leads to an earlier start of the main chamber combustion process (Fig. 9(b)). In turn, this leads to a significant increase in peak cylinder pressure (Fig. 9(a)). The slower end of the main chamber combustion process seems to originate in the lower penetration of the gas jets. It results in a significant increase of the main chamber combustion duration of about 4° CA (Fig. 9(d)).

For the same NO_X emissions, the shift of the main chamber combustion process towards TDC (Fig. 9(b)) fully compensates the detrimental effect of the longer combustion duration (Fig. 9(d)) on the engine fuel economy. Consequently, the reduction of prechamber volume results in no perceptible change in fuel conversion efficiency (Fig. 9(f)). The chemical energy converted into heat in the prechamber produces a sufficiently large increase in pressure (Fig. 9(c)) to generate the hot gas jets required for the main chamber igni-

tion. However, this pressure increase does not directly affect the main chamber pressure (Fig. 9(a)) and thus does not produce mechanical work. The insensitivity of the fuel conversion efficiency to the variation of the prechamber volume indicates that the detrimental effect of burning a larger quantity of fuel in the prechamber without producing mechanical work is fully compensated by the acceleration of the main chamber combustion process realised by the resulting stronger gas jets. The significant improvement of the cycle-by-cycle variability associated with the small prechamber (b) permits an increase in the relative air to fuel ratio, which enables a further reduction of the NO_X emissions. The significant lower cycle-by-cycle variability associated with the small prechamber may originate in the lower turbulence in the vicinity of the spark plug electrodes indicated by the numerical simulation ([1], Fig. 11(b), lowest graph).

Despite a better combustion stability which tends to reduce the contribution of bulk gas quenching, the reduction of the prechamber internal volume yields more than ≈7% and ≈11% higher CO and THC emissions at constant NO_X emissions (Fig. 9(e)). This tends to indicate that the increase in CO and THC emissions mainly results from the combustion chamber crevice mechanisms. On the one hand, the higher peak cylinder pressure tends to increase the amount of unburnt mixture flowing into the combustion chamber crevices. On the other hand, weaker gas jets are likely to delay the arrival of the flame front at the entrance of the piston top land and cylinder head gasket crevices. Both effects tend to increase the amount of hydrocarbons escaping the primary oxidation process. The reduction of the prechamber internal volume also causes a more rapid increase of the THC emissions and a fundamental change in the evolution of the CO emissions with the increase in relative air to fuel ratio. This particular behaviour tends to indicate that the intensity and penetration of the gas jets has a major influence on the exhaust gas emissions.

3.6. Prechamber internal shape

A first insight into the influence of the prechamber internal shape was gained on the basis of two different geometries. In order to enable a sufficient variation of the internal shape without modification of the prechamber external geometry, this study was based on the small prechamber volume of 3010 mm^3. The first internal shape corresponds to the case *b* represented in Fig. 1(b). The second internal shape (c) was designed in order to distribute more uniformly the volume along the prechamber axis. With a size of 14 mm, the larger diameter of the upper prechamber part corresponds to the thread dimensions of the standard spark plug used. Derived from the internal shape *b*, the length between the point where the nozzle orifice axes converge and the prechamber top face (prechamber length) as well as the prechamber cone angle were kept constant. The investigation was carried out with prechambers featured with 6 nozzle orifices of diameter 1.63 mm ($A_n = 12.52$ mm^2), unevenly distributed and oriented at ≈78°. The engine was operated at a constant spark timing of 8.3° CA_{BTDC}.

The results corresponding to the two different prechamber internal shapes are shown in Fig. 10. The transition from internal shape *b* to *c* leads to a delay of the prechamber pressure pulse and a decrease of its intensity (Fig. 10(c)). The longer pressure pulse observed with shape *c* results from the larger main chamber ignition delay (Fig. 10(d)). The slower and less intense prechamber combustion process is expected to delay the development of the gas jets in the main chamber and attenuates their intensity and penetration. When considering the same relative air to fuel ratio, this leads to an important increase in main chamber ignition delay of approximately 3° CA. In turn, this results in a shift of the main chamber combustion process into the expansion phase (Fig. 10(d)). The less efficient combustion requires a larger mass flow rate of fuel-air mixture in order to achieve a constant engine power output, which results in an higher compression pressure (Fig. 10(a)) and heat release integral (Fig. 10(b)). Further, the shift of the main combustion process into the expansion phase yields a significant decrease in peak combustion pressure, which becomes much smaller than the maximum value reached during compression (Fig. 10(a)).

In comparison to the prechamber with internal shape *b*, the slower and later main chamber combustion process induced by internal shape *c* enables a reduction of the relative air to fuel ratio to achieve the same NO_X emissions (Fig. 10(e)). At equal NO_X emissions, the shift of the main chamber combustion process into the expansion phase produced by internal shape *c* causes a significant decrease of more than 0.5%-point in fuel conversion efficiency (Fig. 10(f)). Despite the slight decrease in relative air to fuel ratio, the later and slower combustion process associated with the shape *c* causes a significant increase in cycle-by-cycle variability, which is illustrated by a higher coefficient of variance of p_{mi}.

When considering equal NO_X emissions, the change from shape *b* to *c* yields ≈11% and ≈13% lower CO and THC emissions, respectively (Fig. 10(e)). This result is expected to mainly originate in the significantly lower combustion pressure characterising shape *c*, which tends to reduce the amount of unburnt mixture compressed in the combustion chamber crevices and thus escaping the primary oxidation process.

The engine operation with the prechamber internal shape *c* yields approximately the same CO and THC emissions as with the large prechamber (shape *a*), at constant NO_X emissions. On the other hand, shape *c* enables a further reduction of the NO_X emissions. However, it also leads to a decrease in fuel conversion efficiency of more than 0.5%-point. Further, the effective potential to reduce the NO_X emissions sufficiently under the Swiss limits to be practical is strongly limited by the simultaneous increase of the CO emissions. In this respect, the significantly more stable behaviour of the CO emissions characterising the

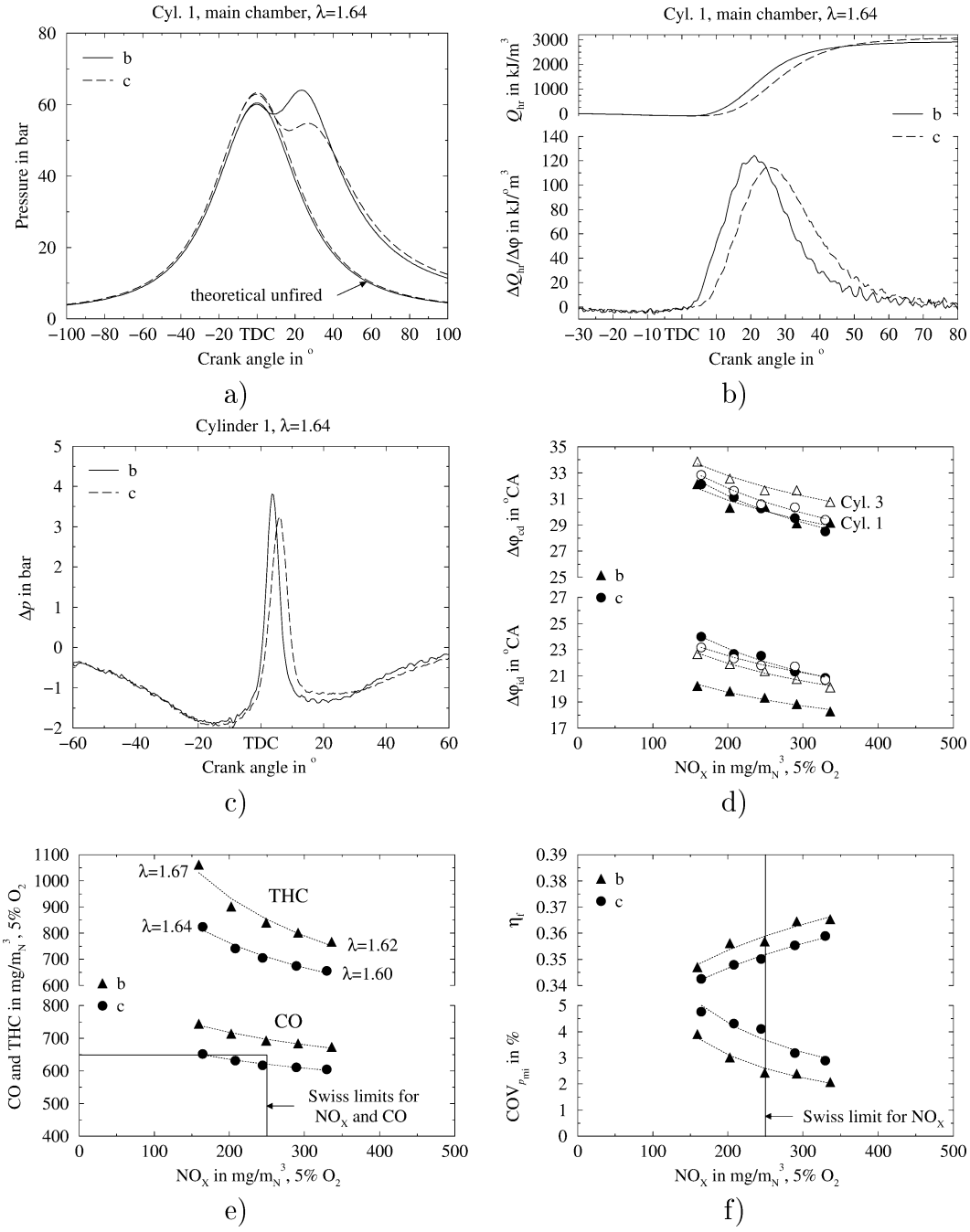

Fig. 10. Influence of the prechamber internal shape on the engine performance and emissions: main chamber pressure (a), main chamber heat-release rate and integral (b) and pressure difference between pre- and main chamber (c) at constant relative air to fuel ratio; ignition delay and combustion duration (d) CO and THC emissions (e) and fuel conversion efficiency and coefficient of variance of p_{mi} (f) as function of NO_X emissions; $V_{\mathrm{p}} = 3010\ \mathrm{mm}^3$, $N_{\mathrm{n}} = 6$, $A_{\mathrm{n}} = 12.52\ \mathrm{mm}^2$, $\alpha_{\mathrm{n}} \approx 78°$, $\mathrm{ST} = 8.3°\ \mathrm{CA}_{\mathrm{BTDC}}$, NG6.

engine operation with the large prechamber offers, at this stage, more potential to reduce the CO emissions to an adequate level under the Swiss limits, while keeping the highest possible fuel conversion efficiency.

4. Conclusions

The prechamber geometrical parametric study indicates that the following trends have a beneficial effect on the penetration of the gas jets and/or promote an early arrival of the flame front at the piston top land and cylinder head gasket crevice entrances.

- a small total nozzle orifice cross sectional area. However, the reduction of this area is limited by the occurrence of ignition failure, likely to result from an excessive increase in turbulence intensity at the ignition point. There is an optimum area, which enables mini-

mum NO_X emissions to be achieved for a given nozzle orifice configuration;
- a limited number of nozzle orifices (4 instead of 6);
- an orientation of the nozzle orifices towards the squish region ($\approx$78° instead of $\approx$62°);
- a relatively large prechamber internal volume (2.9 instead of 1.9% of V_c).

This limits the amount of unburnt mixture escaping the primary oxidation process and consequently reduces significantly the CO and THC emissions. Further, these trends increase slightly or do not affect the fuel conversion efficiency.

On the other hand, the investigation of the nozzle orifice azimuthal distribution indicates no clear trend regarding the CO and THC emissions. However, these results are based on a prechamber with 6 orifices and are therefore not necessarily valid for a smaller number of orifices. Further, the parametric study shows a large influence of the prechamber internal shape.

Acknowledgements

This research work was carried out at the *Laboratory for Industrial Energy Systems* (*LENI*) of the *Swiss Federal Institute of Technology of Lausanne* (*EPFL*). It was financially supported by the *Swiss Federal Office of Energy* (*OFEN*), under the grant no 69 801, the engine manufacturer *Liebherr Machines Bulle S.A.*, the cogeneration group manufacturer *Dimag S.A.*, the *Research Fund of the Gas Industry* (*FOGA*), as well as by the *EPFL*, who are all gratefully acknowledged.

References

[1] R.-P. Roethlisberger, D. Favrat, Investigation of the prechamber geometrical configuration of a natural gas spark ignition engine for cogeneration. Part I. Numerical simulation, Internat. J. Therm. Sci. 42 (3) (2003), to appear.

[2] J.-B. Heywood, Internal Combustion Engine Fundamentals, in: International Editions, Automotive Technology Series, McGraw-Hill, New York, 1988.

[3] R.-P. Roethlisberger, G. Leyland, C.-A. Paschoud, D. Favrat, Swiss Motor, Modification d'un moteur Diesel pour le fonctionnement avec mélange stœchiométrique ($\lambda = 1$) et pauvre ($\lambda \gg 1$), Swiss Federal Office of Energy, Final Report, 1998.

[4] R.-P. Roethlisberger, G. Leyland, D. Favrat, R.-R. Raine, Study of a small size cogeneration gas engine in stoichiometric and lean burn modes: Experimentation and simulation, SAE Paper 982451 and SP-1391, 1998.

[5] R.-P. Roethlisberger, R.-R. Raine, R. Kleemann, D. Favrat, Experimental results and modelling of carbon monoxide emissions from a natural gas fuelled spark-ignition cogeneration engine, in: IMechE International Conference on Computational and Experimental Methods in Reciprocating Engines, IMechE Conference Transactions, 2000, pp. 127–138, ISBN 1-86058-275-3.

[6] R.-P. Roethlisberger, An experimental investigation of a lean burn natural gas prechamber spark ignition engine for cogeneration, Swiss Federal Institute of Technology of Lausanne, Ph.D. Thesis n^o 2346, 2001, also published under Swiss Motor, Modification d'un moteur diesel pour le fonctionnement au gaz naturel en cogeneration, fonctionnement avec préchambre de combustion, Swiss Federal Office of Energy, Final Report, 2001 (in English).

[7] R. Kuratle, Motorenmeßtechnik, Vogel Fachbuch, 1995, ISBN 3-8023-1553-7.

[8] N. Chigier, Energy, Combustion and Environment, in: Energy, Combustion and Environment Series, McGraw-Hill, New York, 1981, ISBN 0-07-010766-1.